A phenomenological model for the rare-earth contribution to the magnetic anisotropy in $RFe_{11}Ti$ and $RFe_{11}TiH$

2006 J. Phys.: Condens. Matter 18 221

(http://iopscience.iop.org/0953-8984/18/1/016)

INSTITUTE OF PHYSICS PUBLISHING JOURNAL OF PHYSICS: CONDENSED MATTER

J. Phys.: Condens. Matter **18** (2006) 221–242 doi:10.1088/0953-8984/18/1/016

A phenomenological model for the rare-earth contribution to the magnetic anisotropy in $RFe_{11}Ti$ and $RFe_{11}TiH$

Cristina Piquer[1], Fernande Grandjean[2], Olivier Isnard[3,4] and Gary J Long[5]

[1] Instituto de Ciencia de Materiales de Aragón–CSIC, Universidad de Zaragoza, E-50009 Zaragoza, Spain
[2] Department of Physics, B5, University of Liège, B-4000 Sart-Tilman, Belgium
[3] Laboratoire de Cristallographie, CNRS, associé à l'Université J. Fourier, BP 166X, F-38042 Grenoble Cedex, France
[4] Institut Universitaire de France, Maison des Universités, 103 Boulevard Saint-Michel, F-75005 Paris, Cedex, France
[5] Department of Chemistry, University of Missouri-Rolla, Rolla, MO 65409-0010, USA

E-mail: cpiquer@unizar.es, fgrandjean@ulg.ac.be, olivier.isnard@grenoble.cnrs.fr and glong@umr.edu

Received 21 July 2005
Published 9 December 2005
Online at stacks.iop.org/JPhysCM/18/221

Abstract

A phenomenological model based on the interactions between the crystal field and the 3d–4f exchange interactions has been developed to explain the zero-kelvin magnetic anisotropy of the $RFe_{11}Ti$ compounds and their hydrides, $RFe_{11}TiH$, where R is a rare-earth element. In most cases, this model also predicts the existence of a spin reorientation either in the $RFe_{11}Ti$ or the $RFe_{11}TiH$ compounds. A more advanced model, that takes into account the temperature dependence of the anisotropy coefficient, expressed in terms of generalized Brillouin functions, has also been developed and used to predict the spin-reorientation temperatures of several of the compounds. A set of crystalline electric field parameters for the $RFe_{11}Ti$ and $RFe_{11}TiH$ compounds, with R = Pr, Nd, Sm, Tb, Dy, Ho and Er, has been obtained. With these parameters the magnetic phase diagrams of the $RFe_{11}Ti$ and $RFe_{11}TiH$ compounds have been reproduced. More specifically, the spin-reorientation temperatures and the temperature dependence of the magnetocrystalline anisotropy are correctly predicted when the higher-order terms of the crystal field are included in the model. Further, changes in the magnetocrystalline anisotropy that take place upon hydrogenation have been explained by a substantial decrease in the first-order crystal field coefficient, A_{20}, accompanied by a smaller decrease of the third-order coefficient, A_{60}. $ErFe_{11}TiH$ and $NdFe_{11}TiH$ exhibit a smaller decrease in their A_{nm} parameters upon hydrogenation than do the remaining rare-earth compounds.

(Some figures in this article are in colour only in the electronic version)

1. Introduction

The series of $RFe_{11}Ti$ compounds and their hydrides, $RFe_{11}TiH$, where R is a rare-earth element, all of which crystallize [1, 2] in the $ThMn_{12}$ structure with the $I4/mmm$ space group, exhibit a wide variety of magnetic behaviours [3–5]. For instance they exhibit different easy magnetization directions and spin-reorientation transitions, depending on both the rare-earth element and/or the presence of hydrogen [6–8]. Several authors have systematically been studying [9–21] the magnetic and Mössbauer spectral properties of the $RFe_{11}Ti$ and $RFe_{11}TiH$ compounds, where R is Ce, Pr, Nd, Sm, Gd, Tb, Dy, Ho, Er and Lu, between 4.2 and 295 K.

The unit-cell volumes and some of the magnetic properties [10, 11, 14–17, 20, 22, 23] of the $RFe_{11}Ti$ and $RFe_{11}TiH$ compounds are summarized in table 1. The insertion of hydrogen into $RFe_{11}Ti$ to form $RFe_{11}TiH$ produces a significant increase in both the Curie temperature, T_c, and the saturation magnetization, M_s. The presence of interstitial hydrogen also induces significant changes in the magnetocrystalline anisotropy [6, 8, 10, 19, 22, 24–26] of the parent compound. The easy magnetization direction in the $RFe_{11}Ti$ and $RFe_{11}TiH$ compounds at 4.2 and 295 K are also given in table 1. The Mössbauer spectra have all been consistently analysed with a model that considers both the easy magnetization direction and the distribution of titanium in the near-neighbour environment of the three crystallographically inequivalent iron sites in the compounds. The earlier, different, analysis [9] of the Mössbauer spectra of $CeFe_{11}Ti$ and $CeFe_{11}TiH$ is revised in a companion paper [18] to this paper. Extensive information has been obtained on both the magnetic anisotropy and the spin reorientations exhibited by these compounds. Hence, it is worthwhile to rationalize this extensive new information in terms of an internally consistent magnetic model.

In the rare-earth–iron intermetallic compounds the total magnetocrystalline anisotropy results from the contributions of both the rare-earth and iron sublattices. The iron sublattice contribution to the total magnetocrystalline anisotropy is always axial and generally dominates at high temperatures. The rare-earth sublattice contribution, which usually dominates at low temperatures, is essentially determined by both the crystalline electric field experienced by the rare-earth ion and the exchange interactions between the sublattices. The contribution of the rare-earth sublattice to the magnetic anisotropy may be different for each rare earth and may vary with temperature. A spin reorientation will occur when the balance of the iron and rare-earth sublattice contributions to the magnetic anisotropy changes with temperature. The insertion of hydrogen in rare-earth–iron intermetallic compounds usually has a dramatic effect on the macroscopic magnetocrystalline anisotropy. In particular, in the $RFe_{11}Ti$ compounds hydrogenation decreases the spin-reorientation temperature in $NdFe_{11}Ti$ and $ErFe_{11}Ti$, suppresses the spin-reorientation temperature in $TbFe_{11}Ti$ and $DyFe_{11}Ti$ and induces the appearance of a spin reorientation in going from $HoFe_{11}Ti$ to $HoFe_{11}TiH$, see table 1.

Several authors [4, 23, 27–29] have modelled the interactions between the crystal field and the 3d–4f exchange in order to explain the magnetic anisotropies of specific $RFe_{11}Ti$ and $RFe_{11}TiH$ compounds. However, except for the work of Isnard [8], there has been no systematic study of the influence of the interstitial hydrogen on the macroscopic magnetocrystalline anisotropy.

Herein we present a detailed study of the macroscopic magnetocrystalline anisotropy of the $RFe_{11}Ti$ and $RFe_{11}TiH$ compounds and obtain a systematic and quantitative evaluation of the influence of hydrogenation upon the magnetic and crystal field interactions. To accomplish this, we have used, first, a phenomenological model for the magnetocrystalline anisotropy of the $RFe_{11}Ti$ and $RFe_{11}TiH$ compounds at zero kelvin, see section 2, and, second, a model which accounts for the temperature dependence of the magnetic anisotropy and the spin-reorientation transitions observed in these compounds, see section 3.1.

Table 1. The crystallographic and magnetic properties of the $RFe_{11}Ti$ and $RFe_{11}TiH$ compounds.

Compound	V (Å^3)[a]	T_c (K)	T_s (K)	EMD$^{300\ K}$	EMD$^{4.2\ K}$	$M_s^{300\ K}$ (μ_B/f.u.)	$M_s^{5\ K}$ (μ_B/f.u.)	Ref.
$CeFe_{11}Ti$	348.5	487	—	Axial	Axial	15.0	17.4	[22]
$CeFe_{11}TiH$	352.5	542	—	Axial	Axial	15.3	17.6	[22]
$PrFe_{11}Ti$	355.6	547	—	Basal	Basal	19.2	16.8	[16]
$PrFe_{11}TiH$	357.1	604	—	Basal	Basal	20.5	19.3	[16]
$NdFe_{11}Ti$	352.4	551	200	Axial	Canted	20.1	21.9	[15]
$NdFe_{11}TiH$	354.7	614	125	Axial	Basal	21.6	24.0	[15]
$SmFe_{11}Ti$	350.8	591	—	Axial	Axial	17.3	19.3	[17]
$SmFe_{11}TiH$	353.4	634	—	Axial	Axial	18.2	19.3	[17]
$GdFe_{11}Ti$	349.2	621	—	Axial	Axial	13.5	14.8	[22]
$GdFe_{11}TiH$	351.8	652	—	Axial	Axial	14.7	15.7	[22]
$TbFe_{11}Ti$	347.3	578	338	Basal	Basal	11.7	10.5	[14]
$TbFe_{11}TiH$	351.0	620	—	Basal	Basal	12.2	11.3	[14]
$DyFe_{11}Ti$	347.5	552	100, 200	Axial	Basal	12.0	10.0	[23]
$DyFe_{11}TiH$	350.3	600	—	Basal	Basal	12.9	10.9	[23]
$HoFe_{11}Ti$	344.9	533	—	Axial	Axial	14.0	10.1	[11]
$HoFe_{11}TiH$	348.4	590	150	Axial	Canted	14.7	10.6	[11]
$ErFe_{11}Ti$	344.1	518	50	Axial	Canted	12.9	9.8	[10]
$ErFe_{11}TiH$	347.6	574	40	Axial	Basal(?)	12.9	10.6	[10]
$LuFe_{11}Ti$	342.2	498	—	Axial	Axial	15.2	16.0	[17]
$LuFe_{11}TiH$	345.7	558	—	Axial	Axial	15.3	17.2	[17]

[a] The unit-cell volume whose error is approximately ±1 in the last digit.

2. Phenomenological model for the magnetocrystalline anisotropy at zero kelvin

The magnetic anisotropy energy of a rare-earth ion in the tetragonal symmetry observed for both the $RFe_{11}Ti$ and $RFe_{11}TiH$ compounds, may be described at zero kelvin by the phenomenological expression

$$E_R^a = K_{1R}\sin^2\theta + [K_{2R} + K'_{2R}\cos 4\phi]\sin^4\theta + [K_{3R} + K'_{3R}\cos 4\phi]\sin^6\theta, \tag{1}$$

where θ and ϕ are the angles between the magnetization and the tetragonal [001] and basal [100] axes, respectively; the remaining parameters are defined below. The relationship [30] between the anisotropy coefficients, K_{iR}, and the crystal field parameters, B_{nm}, are given by the expressions

$$K_{1R} = -(3/2)B_{20}\langle O_{20}\rangle - 5B_{40}\langle O_{40}\rangle - (21/2)B_{60}\langle O_{60}\rangle, \tag{2a}$$

$$K_{2R} = (35/8)B_{40}\langle O_{40}\rangle + (189/8)B_{60}\langle O_{60}\rangle, \tag{2b}$$

$$K_{3R} = -(231/16)B_{60}\langle O_{60}\rangle, \tag{2c}$$

$$K'_{2R} = (1/8)B_{44}\langle O_{40}\rangle + (5/8)B_{64}\langle O_{60}\rangle \tag{2d}$$

and

$$K'_{3R} = -(11/16)B_{64}\langle O_{60}\rangle, \tag{2e}$$

where $\langle O_{nm}\rangle$ are the thermal averages of the Stevens operators [31] and B_{nm} are the crystal field parameters, which depend on the rare-earth ion, and are given by $B_{nm} = \theta_n A_{nm}\langle r^n\rangle$, where θ_n are the single-ion Stevens coefficients, $\theta_2 = \alpha_J$, $\theta_4 = \beta_J$ and $\theta_6 = \gamma_J$, A_{nm} are the crystal field coefficients and $\langle r^n\rangle$ are the average values of the 4f electronic radial distributions.

The easy magnetization direction is determined by the total magnetic anisotropy energy,

$$E_{tot}^a = E_R^a + K_{1Fe}\sin^2\theta, \tag{3}$$

which has contributions from the rare earth and iron. From equations (1) to (3), one observes, for instance see [29], that a compound has an axial magnetization, i.e., $\theta = 0$, if both of the following inequalities are fulfilled:

$$K_{1\mathrm{Fe}} + K_{1\mathrm{R}} > 0 \tag{4a}$$

and

$$K_{1\mathrm{Fe}} + K_{\mathrm{eff,R}} > 0, \tag{4b}$$

where $K_{\mathrm{eff,R}}$ is defined by the expression

$$K_{\mathrm{eff,R}} = K_{1\mathrm{R}} + K_{2\mathrm{R}} + K_{3\mathrm{R}} - |K'_{2\mathrm{R}} + K'_{3\mathrm{R}}|. \tag{4c}$$

In many intermetallic rare-earth–transition metal compounds, the rare-earth contribution to the total magnetocrystalline anisotropy is described by using only the second-order crystal field term. However, in the $RFe_{11}Ti$ compounds and their hydrides, this approximation is inadequate because the second-order crystal field coefficient, A_{20}, is relatively small in the $ThMn_{12}$ structure. Hence the fourth-order and sixth-order crystal field terms play an important role and must be taken into account [3, 4, 8] in determining the magnetocrystalline anisotropy contribution from the rare-earth sublattice. For the $RFe_{12-x}M_x$ compounds, A_{20} and A_{40} are known [20, 32–34] to be negative, whereas A_{60} is positive. Consequently, the first term in $K_{1\mathrm{R}}$ is negative and favours an axial anisotropy contribution from the rare earths with $\alpha_J > 0$, i.e., for Er and Sm, whereas it is positive and favours a basal contribution from the rare earths with $\alpha_J < 0$, i.e., for Pr, Nd, Tb, Dy and Ho. Similarly, the second term in $K_{1\mathrm{R}}$ gives an axial contribution when $\beta_J > 0$, i.e., for Er, Tb and Sm, and the third term of $K_{1\mathrm{R}}$ gives an axial contribution when $\gamma_J < 0$, i.e., for Nd, Ho and Tb.

The different terms in equations (2) and (4) can easily be calculated at zero kelvin if the B_{nm} parameters are known. The values of θ_n, $\langle r^n \rangle$ and $\langle O_{nm} \rangle$ at zero kelvin are tabulated in the literature [35, 36]. Figure 1 shows the product $\theta_n \langle r^n \rangle \langle O_{nm} \rangle$ at zero kelvin as a function of the atomic number of the rare earth and will be helpful in the following discussion. In contrast, unfortunately, there is an important variation in the literature values of the A_{nm} parameters, a variation that results from the different approximations used by different authors and may also come from differing stoichiometry of the $RFe_{11}Ti$ compounds under study. We believe that the most reliable method for determining the A_{nm} parameters of a given compound is from the fit of the single-crystal magnetization curves with the mean field approximation including exchange and crystal field interactions, see [27, 28, 37]. Unfortunately, to the best of our knowledge, a relevant set of crystal field parameters has been reported [27, 28] using this method only for $DyFe_{11}Ti$, $HoFe_{11}Ti$ and $TbFe_{11}Ti$. From the single-crystal magnetization analysis of $DyFe_{11}Ti$, Hu *et al* [28] have obtained $A_{20} = -32.3\ \mathrm{K}a_0^{-2}$, $A_{40} = -12.4\ \mathrm{K}a_0^{-4}$, $A_{60} = 2.56\ \mathrm{K}a_0^{-6}$, $A_{44} = 118\ \mathrm{K}a_0^{-4}$ and $A_{64} = 0.64\ \mathrm{K}a_0^{-6}$, where a_0 is the Bohr radius. Abadia *et al* [27] have obtained $A_{20} = -20.5\ \mathrm{K}a_0^{-2}$, $A_{40} = -11.1\ \mathrm{K}a_0^{-4}$, $A_{60} = 5.02\ \mathrm{K}a_0^{-6}$, $A_{44} = -153.2\ \mathrm{K}a_0^{-4}$ and $A_{64} = -0.81\ \mathrm{K}a_0^{-6}$ from the single-crystal magnetization analysis of $HoFe_{11}Ti$. Although the crystal field coefficients obtained for $HoFe_{11}Ti$ [27] and for $DyFe_{11}Ti$ [28] are similar, the A_{nm} coefficients obtained for $DyFe_{11}Ti$ by Hu *et al* [28] cannot explain [29] the spin-reorientation transition observed in $TbFe_{11}Ti$ and $TbFe_{11.35}Nb_{0.65}$. A more reliable set of crystal field parameters, very different from those reported by Hu *et al* [28] are the values obtained for $TbFe_{11}Ti$ by Abadia *et al* [27] of $A_{20} = -52.5\ \mathrm{K}a_0^{-2}$, $A_{40} = -0.27\ \mathrm{K}a_0^{-4}$, $A_{60} = 0.021\ \mathrm{K}a_0^{-6}$, $A_{44} = -0.0087\ \mathrm{K}a_0^{-4}$ and $A_{64} = -8.9\ \mathrm{K}a_0^{-6}$, which yield a satisfactory explanation of the observed experimental magnetization. The origin of the discrepancy between the different authors is not clear. According to Abadia *et al* [27], an anomalous value of A_{20} has also been obtained for Pr and Yb in their $R_2Fe_{14}B$ compounds

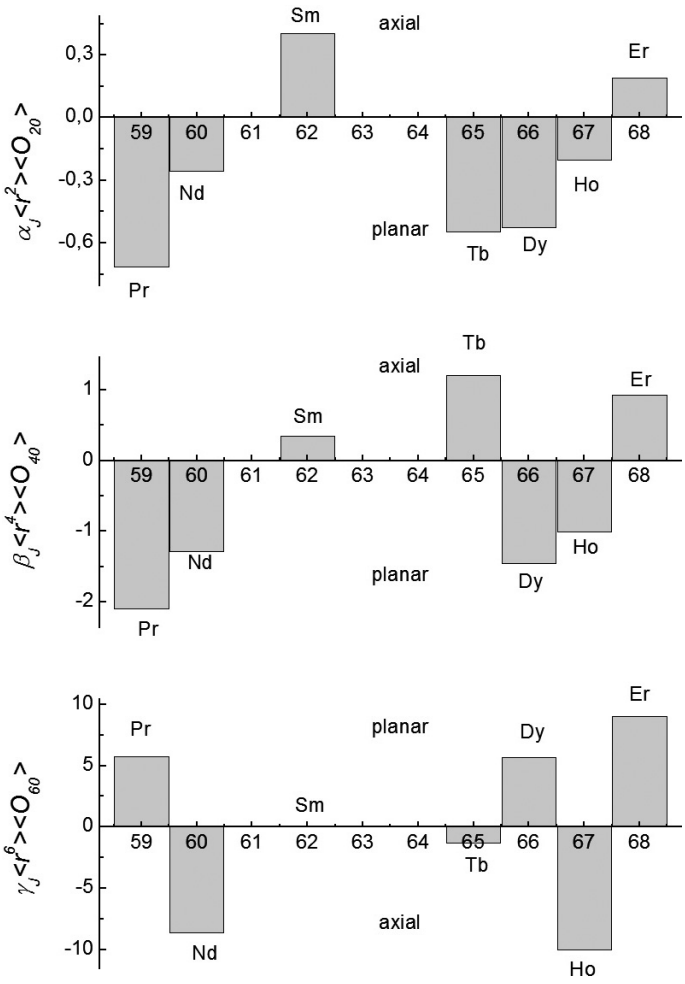

Figure 1. The product $\theta_n \langle r^n \rangle \langle O_{nm} \rangle$, in K, expected at zero kelvin as a function of the atomic number of the rare earth.

and the anomaly has been attributed to an incipient rare-earth valence instability. For the $RFe_{11}TiH$ compounds, a relevant set of crystal field parameters obtained from single-crystal magnetization measurements has been reported [23] only for $HoFe_{11}TiH$ as $A_{20} = -118\ \mathrm{K}a_0^{-2}$, $A_{40} = -8.6\ \mathrm{K}a_0^{-4}$, $A_{60} = 1.4\ \mathrm{K}a_0^{-6}$, $A_{44} = -200\ \mathrm{K}a_0^{-4}$ and $A_{64} = -0.85\ \mathrm{K}a_0^{-6}$.

Because for the remaining rare-earth elements, there are only less reliable reports of A_{nm} parameters obtained from other methods [3, 4, 38–41] than from the fit of single-crystal magnetization curves, the usual procedure [28, 29] is to use the A_{nm} parameters obtained for other $RFe_{11}Ti$ compounds to predict the magnetization direction at zero kelvin. Herein, a similar approach has been used for the $RFe_{11}TiH$ compounds. For $TbFe_{11}Ti$, the crystal field parameters obtained by Abadia *et al* [27] have been used and, for the remaining $RFe_{11}Ti$ compounds, the crystal field parameters reported by Hu *et al* [28] for $DyFe_{11}Ti$ or by Abadia *et al* [27] for $HoFe_{11}Ti$ have been initially used. References [27] and [28] use different sign conventions for the A_{44} and A_{64} parameters, however, the sign is irrelevant for the present analysis because $|K'_{2R} + K'_{3R}|$ is used in equation (4*c*). For $HoFe_{11}TiH$, the set of crystal

field parameters reported by Nikitin *et al* [23] has been used whereas, for the remaining $RFe_{11}TiH$ compounds, these parameters have been scaled to predict the stable magnetic phase at zero kelvin. The $B_{nm}\langle O_{nm}\rangle$ crystal field terms at zero kelvin for the $RFe_{11}Ti$ and $RFe_{11}TiH$ compounds, obtained from the A_{nm} parameters reported in the indicated reference, are given in table 2, a table which also gives the corresponding anisotropy coefficients at zero kelvin, obtained using equations (2*a*)–(2*e*).

In the following discussion, for the $RFe_{11}Ti$ compounds, $K_{1Fe}(0)$ is 24 K/f.u. as is observed for $YFe_{11}Ti$ [27] and for the $RFe_{11}TiH$ compounds, $K_{1Fe}(0)$ is 25.8 K/f.u. as is observed for $YFe_{11}TiH$ [42].

$YFe_{11}Ti$, $CeFe_{11}Ti$, $GdFe_{11}Ti$ and $LuFe_{11}Ti$ and their hydrides exhibit [17, 20, 22] an axial magnetocrystalline anisotropy at all temperatures. Because both yttrium and lutetium are non-magnetic rare earths, only the iron sublattice contributes to the total magnetocrystalline anisotropy of $YFe_{11}Ti$ and $LuFe_{11}Ti$ and their hydrides. In $CeFe_{11}Ti$ the magnetic anisotropy is dominated by the iron sublattice contribution. The spherically symmetric $4f^7$ electronic configuration of the gadolinium ion makes no orbital contribution to its moment and thus there is no crystal field interaction. As a consequence, the magnetic anisotropy of $GdFe_{11}Ti$ and $GdFe_{11}TiH$ is also dominated by the iron sublattice [22].

2.1. Application to the $RFe_{11}Ti$ compounds

To predict the stable magnetic phase at zero kelvin of the $RFe_{11}Ti$ compounds we began our analysis using the A_{nm} parameters reported by Abadia *et al* [27]. By using K_{1Fe} equal to 24.0 K/f.u. [27] and the parameters given in table 2, the sum of the iron and rare-earth anisotropy parameters, as given by the left members of the inequalities (4*a*) and (4*b*), are calculated and given in table 3. As is shown in this table, when R is Pr, Tb, Dy and Er, negative values for $K_{1Fe} + K_{1R}$ and $K_{1Fe} + K_{eff,R}$ are obtained. Hence, the A_{nm} parameters reported by Abadia *et al* [27] predict that these compounds are not axial at zero kelvin, in agreement with the experimental results, see table 1. When R is Sm and Ho, the A_{nm} parameters reported in [27] give positive values of $K_{1Fe} + K_{1R}$ and $K_{1Fe} + K_{eff,R}$, and indicate that these compounds are axial at zero kelvin, again in agreement with the experimental observations, see table 1.

The only exception is $NdFe_{11}Ti$. In this case, the A_{nm} coefficients obtained by Abadia *et al* [27] for $HoFe_{11}Ti$ yield positive values of $K_{1Fe} + K_{1R}$ and $K_{1Fe} + K_{eff,R}$, and, hence, predict that $NdFe_{11}Ti$ should exhibit an axial anisotropy at zero kelvin, in disagreement with the experimental observation, see table 1. The A_{nm} values obtained [28] for $DyFe_{11}Ti$ lead to similar positive values of $K_{1Fe} + K_{1R}$ and $K_{1Fe} + K_{eff,R}$, see table 3. This disagreement is quite surprising because Hu *et al* [29] claim that they can predict the spin-reorientation transition and the canting angle with these parameters through a calculation of the energy surface. Another set of A_{nm} parameters has been obtained for $NdFe_{11}Ti$ by Kou *et al* [4] from magnetic measurements on polycrystalline samples, $A_{20} = -40.4\ \mathrm{K}a_0^{-2}$, $A_{40} = -6.9\ \mathrm{K}a_0^{-4}$, $A_{60} = 0.3\ \mathrm{K}a_0^{-6}$, $A_{44} = 36.6\ \mathrm{K}a_0^{-4}$ and $A_{64} = 0\ \mathrm{K}a_0^{-6}$. With these parameters, $K_{1Fe} + K_{1R} = -8.62$ K/f.u. < 0 and $K_{1Fe} + K_{eff,R} = 0.39$ K/f.u. > 0. Hence, this set of crystal field parameters predicts that $NdFe_{11}Ti$ is not axial at zero kelvin, in agreement with the experimental observations.

All these results can be understood by analysing the relative values of the θ_n and A_{nm} parameters. For praseodymium, α_J and β_J are negative, whereas γ_J is positive, see figure 1. Hence, the three terms of K_{1R} in equation (2*a*) favour a basal rare-earth easy magnetization direction. $PrFe_{11}Ti$ is the only compound in the $RFe_{11}Ti$ series in which the rare-earth magnetocrystalline anisotropy dominates at all temperatures below its Curie temperature, a situation quite unexpected because the rare-earth contribution to the total magnetocrystalline

Table 2. $B_{nm}\langle O_{nm}\rangle$, in K, and the anisotropy coefficients, in K/f.u., for $RFe_{11}Ti$ and $RFe_{11}TiH$ used in the phenomenological model for the magnetocrystalline anisotropy at zero kelvin. (Note: the parameters have been calculated using the A_{nm} parameters reported in the indicated reference.)

Compound	$B_{20}\langle O_{20}\rangle$	$B_{40}\langle O_{40}\rangle$	$B_{60}\langle O_{60}\rangle$	$B_{44}\langle O_{40}\rangle$	$B_{64}\langle O_{60}\rangle$	K_{1R}	K_{2R}	K_{3R}	K'_{2R}	K'_{3R}	$K_{eff,R}$	Ref.
$PrFe_{11}Ti$	14.66	23.26	28.88	321.11	−4.66	−441.6	784.2	−417.0	37.2	3.2	−114.9	[27]
$PrFe_{11}TiH$	84.38	18.02	8.06	419.2	−4.89	−301.1	269.2	−116.3	49.3	3.4	−201.1	[23]
$NdFe_{11}Ti$	5.28	14.22	−43.34	196.25	6.99	376.0	−961.6	625.7	28.9	−4.8	16.0	[27]
$NdFe_{11}Ti$	8.33	15.88	−22.10	−151.15	−5.52	140.14	−452.6	319.0	−22.3	3.8	−11.9	[28]
$NdFe_{11}Ti$[a]	10.41	8.84	−2.60	−46.88	0	−32.62	−22.5	37.3	−5.8	0	−23.6	[4]
$NdFe_{11}TiH$	59.94	6.84	−0.71	−60.95	0	−116.5	12.8	10.5	−7.6	0	−100.9	[23]
$SmFe_{11}Ti$	−8.24	−3.76	0	−51.93	0	31.2	−16.5	0	−6.5	0	8.2	[27]
$SmFe_{11}TiH$	−47.45	−2.95	0	−67.8	0	85.7	−12.7	0	−8.5	0	64.5	[23]
$TbFe_{11}Ti$	28.77	−0.324	−0.027	−0.010	11.37	−41.2	−2.0	0.4	7.10	−7.8	−43.6	[27]
$TbFe_{11}TiH$	165.60	−0.25	−0.007	−0.013	11.93	−246.9	−1.28	0.11	7.5	−8.2	−248.8	[23]
$DyFe_{11}Ti$	10.80	16.19	28.31	223.52	−4.56	−394.5	739.7	−408.8	25.1	3.1	−91.7	[27]
$DyFe_{11}TiH$	62.20	12.54	7.89	291.8	−4.79	−238.9	241.4	−114.0	33.5	3.3	−148.3	[23]
$HoFe_{11}Ti$	4.12	11.13	−50.35	153.66	8.12	466.9	−1140.9	727.0	24.3	−5.6	34.2	[27]
$HoFe_{11}TiH$	23.74	8.62	−14.04	206.6	8.52	68.7	−294.0	202.7	30.4	−5.9	−47.1	[23]
$ErFe_{11}Ti$	−3.94	−10.25	45.08	−141.55	−7.27	−416.2	1020.2	−650.9	−22.2	5.0	−64.1	[27]
$ErFe_{11}TiH$	−22.7	−7.94	12.57	−184.8	−7.63	−58.2	262.3	−181.5	−27.9	5.2	−0.12	[23]

[a] Final set of parameters that correctly predict the stable magnetic phase at zero kelvin.

Table 3. The $K_{1Fe} + K_{1R}$ and $K_{1Fe} + K_{eff,R}$ terms for $RFe_{11}Ti$ and $RFe_{11}TiH$ used in the phenomenological model for the magnetocrystalline anisotropy at zero kelvin.

Compound	$K_{1Fe} + K_{1R}$ (K/f.u.)	$K_{1Fe} + K_{eff,R}$ (K/f.u.)	Ref.	Compound	$K_{1Fe} + K_{1R}$ (K/f.u.)	$K_{1Fe} + K_{eff,R}$ (K/f.u.)	Ref.
$PrFe_{11}Ti$	−417.6	−90.8	[27]	$PrFe_{11}TiH$	−275.3	−175.3	[23]
$NdFe_{11}Ti$	400.0	40.0	[27]	$NdFe_{11}TiH$	−90.7	−75.9	[4, 23]
	164.1	12.04	[28]				
	−8.62	0.39	[4]				
$SmFe_{11}Ti$	55.2	33.2	[27]	$SmFe_{11}TiH$	111.5	90.3	[23]
$TbFe_{11}Ti$	−17.2	−19.6	[27]	$TbFe_{11}TiH$	−221.1	−223.0	[23, 27]
$DyFe_{11}Ti$	−370.5	−67.7	[27]	$DyFe_{11}TiH$	−213.1	−122.5	[23]
$HoFe_{11}Ti$	490.9	58.2	[27]	$HoFe_{11}TiH$	94.5	−21.3	[23]
$ErFe_{11}Ti$	−392.2	−40.1	[27]	$ErFe_{11}TiH$	−32.4	25.7	[23]

anisotropy decreases much faster with increasing temperature than does the iron contribution. This predominance results because the three θ_n single-ion coefficients, and consequently, the $\theta_n\langle r^n\rangle\langle O_{nm}\rangle$ and $B_{nm}\langle O_{nm}\rangle$ terms, for praseodymium have exceptionally large absolute values, see figure 1 and table 2. The large values of $B_{nm}\langle O_{nm}\rangle$ may explain why the rare-earth contribution to the total magnetocrystalline anisotropy overwhelms the axial contribution of the iron sublattice at all temperatures below the Curie temperature.

For samarium, α_J and β_J are positive and favour an axial contribution to the net magnetic anisotropy. Hence, an axial magnetization and no spin-reorientation transition are predicted, in agreement with the earlier results reported by Zhang and Wallace [6] and Kaneko *et al* [43]. Similar predictions are made from the A_{nm} parameters reported by Hu *et al* [28].

For terbium, which has the most negative α_J coefficient after praseodymium, only α_J favours basal anisotropy, see figure 1. Consequently, an important basal contribution arising from the terbium sublattice is expected and, indeed, the $B_{20}\langle O_{20}\rangle$ value obtained for $TbFe_{11}Ti$ is larger than the values obtained for any of the other $RFe_{11}Ti$ compounds, see table 2. This large value of $B_{20}\langle O_{20}\rangle$ may explain why the rare-earth contribution to the total magnetocrystalline anisotropy overwhelms [4] the axial contribution below 338 K.

For dysprosium, α_J and β_J are negative and γ_J is positive and, thus, the three terms of K_{1R} favour a basal orientation of the rare-earth magnetization. The anisotropy of dysprosium is very similar to that of praseodymium, i.e., the three terms of K_{1R} favour basal anisotropy, but in $DyFe_{11}Ti$ the $B_{nm}\langle O_{nm}\rangle$ terms are smaller, see table 2. As a consequence, the basal contribution from dysprosium cannot overwhelm the axial iron contribution at all temperatures and a spin-reorientation transition occurs in $DyFe_{11}Ti$.

$HoFe_{11}Ti$ unexpectedly exhibits [3, 11, 45, 46] an axial easy magnetization direction at all temperatures below its Curie temperature of 533 K, because, for holmium, α_J and β_J are negative and hence give basal contributions to the total magnetocrystalline anisotropy, see figure 1. The $B_{nm}\langle O_{nm}\rangle$ calculated from the A_{nm} parameters reported by Abadia *et al* [27], see table 2, show that the sixth-order crystal field term strongly dominates at zero kelvin and is responsible for the large positive values of K_{1R} and $K_{eff,R}$. In other words, $HoFe_{11}Ti$ exhibits an axial magnetic anisotropy because *both* the iron and rare-earth sublattices favour axial anisotropy. The importance of the sixth-order crystal field term was not recognized in earlier work [28] in which the absence of a spin-reorientation transition was ascribed to the dominance of the axial iron anisotropy over the basal holmium anisotropy at all temperatures.

For erbium, α_J and β_J are positive and both the second- and fourth-order crystal field terms favour an axial magnetic anisotropy, see figure 1. However, in $ErFe_{11}Ti$ the $B_{60}\langle O_{60}\rangle$

term is exceptionally large and favours basal anisotropy, see table 2. Consequently, in $ErFe_{11}Ti$ the observed [10, 24] spin-reorientation transition is determined by the sixth-order crystal field term. It is remarkable that, in the cases of Ho and Er, at low temperature, the sixth-order crystal field term dominates but has an opposite sign and, as a consequence, $HoFe_{11}Ti$ is axial and $ErFe_{11}Ti$ is canted below 50 K.

$NdFe_{11}Ti$ undergoes [3, 4, 15, 39] a second-order spin-reorientation transition at 200 K. This transition is not surprising because for neodymium α_J and β_J are negative, see figure 1, and favour a basal magnetic anisotropy. However, both the parameters reported for $HoFe_{11}Ti$ [27] and $DyFe_{11}Ti$ [28] predict that $NdFe_{11}Ti$ should exhibit an axial anisotropy at zero kelvin, in disagreement with the experimental observation. The difference between the predictions from the parameters of Abadia *et al* [27] or Hu *et al* [28] and of Kou *et al* [4] result from the very large $\gamma_J\langle r^6\rangle\langle O_{60}\rangle$ term for $NdFe_{11}Ti$, see figure 1. By using the A_{nm} parameters from [27] or [28], the $B_{60}\langle O_{60}\rangle$ term, i.e., the axial contribution of the neodymium, is exceptionally large for $NdFe_{11}Ti$, see table 2. In contrast, Kou *et al* [4] have reported an A_{60} parameter which is *an order of magnitude* lower than those reported by Abadia *et al* [27] or by Hu *et al* [28]. Consequently, the axial contribution to the net rare-earth anisotropy is greatly reduced, see table 2, and these parameters predict that the $NdFe_{11}Ti$ is not in an axial magnetic phase at zero kelvin.

Summarizing, the A_{nm} parameters reported for $HoFe_{11}Ti$ [27] and $DyFe_{11}Ti$ [28] correctly predict the stable magnetic phase at zero kelvin for the $RFe_{11}Ti$ compounds when R is Pr, Sm, Dy, Ho and Er. As has previously been noted, these parameters do not predict the stable magnetic phase at zero kelvin for $TbFe_{11}Ti$ [28, 29]. In this case, the correct magnetic phase at zero kelvin is correctly obtained by using the A_{nm} parameters reported by Abadia *et al* [27]. The most surprising result concerns $NdFe_{11}Ti$ for which neither of the previously reported [27, 28] A_{nm} parameters predict the correct magnetic phase at zero kelvin. In this case, the magnetic phase at zero kelvin can be obtained by using the crystal field parameters reported by Kou *et al* [4], parameters which give a significantly reduced axial contribution to the net rare-earth anisotropy.

2.2. *Application to the $RFe_{11}TiH$ compounds*

It is well established from gadolinium-155 Mössbauer spectral measurements [20] that the A_{20} parameter becomes more negative in going from $GdFe_{11}Ti$ to $GdFe_{11}TiH$. Hence, to a first approximation, there is an increase in the rare-earth contribution to the magnetic anisotropy, an increase that has been confirmed by high-field magnetization measurements [19, 22, 24] on $SmFe_{11}Ti$ and $ErFe_{11}Ti$.

For the $RFe_{11}TiH$ compounds, where R is Pr, Sm, Dy, Ho and Er, we use the A_{nm} parameters reported by Nikitin *et al* [23] for $HoFe_{11}TiH$ to predict the stable magnetic phase at zero kelvin. For $TbFe_{11}TiH$ and $NdFe_{11}TiH$ the A_{nm} parameters are assumed to vary upon hydride formation in a fashion similar to the variation observed for $HoFe_{11}Ti$. In going from $HoFe_{11}Ti$ to $HoFe_{11}TiH$, the relative variations, Δ_{20}, Δ_{40}, Δ_{60}, Δ_{44} and Δ_{64}, of A_{20}, A_{40}, A_{60}, A_{44} and A_{64}, are 4.75, −0.22, −0.72, 0.30 and 0.05, respectively. By assuming that $A_{nm}(1) = A_{nm}(0) + \Delta_{nm}A_{nm}(0)$, where $A_{nm}(1)$ and $A_{nm}(0)$ are the parameters for the $RFe_{11}TiH$ and $RFe_{11}Ti$, respectively, a set of A_{nm} parameters is easily obtained for the $RFe_{11}TiH$ compounds. The corresponding $B_{nm}\langle O_{nm}\rangle$ parameters and the phenomenological anisotropy coefficients, $K_{i\mathrm{R}}$, are given in table 2. As may be observed in this table, upon hydride formation, there is both an important increase in the absolute value of A_{20}, or equivalently in $B_{20}\langle O_{20}\rangle$, and a significant concomitant reduction in the absolute value of the sixth-order term, $B_{60}\langle O_{60}\rangle$.

By using K_{1Fe} equal to 25.8 K/f.u. [42] and the parameters given in table 2, the anisotropy parameters given by equations (4*a*) and (4*b*) have been obtained and are given in table 3. As may be seen in this table, $SmFe_{11}TiH$ is predicted to be axial [6, 19] and the $RFe_{11}TiH$ compounds, where R is Pr, Nd, Tb, Dy, Ho and Er, are predicted to be non-axial at zero kelvin, in agreement with experimental results [8, 10, 11, 13–16, 22, 47]. Hence, in the framework of the phenomenological model of the magnetocrystalline anisotropy, the variation upon hydrogenation of the crystal field parameters reported for $HoFe_{11}TiH$ can reproduce the stable magnetic phase of the $RFe_{11}TiH$ compounds at zero kelvin. Moreover, for the $RFe_{11}TiH$ compounds, where R is Pr, Sm, Tb, Dy and Ho, the experimentally observed hydrogen induced modifications of the magnetocrystalline anisotropy can be understood in terms of the observed variations in the A_{nm} parameters of $HoFe_{11}Ti$. However the situation becomes more complex for the $RFe_{11}TiH$ compounds when R is Nd and Er, as will be discussed below.

In $PrFe_{11}TiH$ no change in the total magnetocrystalline anisotropy is observed upon hydrogenation, and the easy magnetization direction lies within the basal plane between 4.2 K and the Curie temperature [16]. Consequently, even though K_{1Fe} increases slightly upon hydrogenation and $B_{60}\langle O_{60}\rangle$ decreases, $B_{20}\langle O_{20}\rangle$ markedly increases and, as a consequence, the rare-earth contribution to the anisotropy remains dominant at all temperatures.

For $TbFe_{11}Ti$, $DyFe_{11}Ti$ and $HoFe_{11}Ti$, in agreement with previous observations on other rare earths, we have experimentally observed [8, 11, 13, 14] that hydrogenation reinforces the rare-earth contribution to the total magnetocrystalline anisotropy. As is shown in table 2 for $TbFe_{11}TiH$, the $B_{20}\langle O_{20}\rangle$ term, which gives a basal contribution to the rare-earth anisotropy, is larger than for the other $RFe_{11}TiH$ compounds. Further, the axial $B_{40}\langle O_{40}\rangle$ and $B_{60}\langle O_{60}\rangle$ contributions are negligible in $TbFe_{11}TiH$. Hence, it seems reasonable that in $TbFe_{11}TiH$ the basal rare-earth contribution to the total magnetocrystalline anisotropy overwhelms the axial contribution of the iron sublattice at all temperatures below the Curie temperature of 620 K. The behaviour is similar for $DyFe_{11}TiH$ in which the observed increase in the basal $B_{20}\langle O_{20}\rangle$ term enhances the dysprosium magnetic anisotropy which then dominates that of iron below the Curie temperature of 600 K. In $HoFe_{11}Ti$ the most remarkable change upon hydrogenation is the less negative axial $B_{60}\langle O_{60}\rangle$ contribution. Indeed, in $HoFe_{11}Ti$ the sixth-order term dominates at zero kelvin and the net contribution of the holmium sublattice favours axial magnetocrystalline anisotropy. Because in $HoFe_{11}TiH$ the $B_{60}\langle O_{60}\rangle$ axial contribution is significantly smaller, see table 2, the basal $B_{20}\langle O_{20}\rangle$ and $B_{40}\langle O_{40}\rangle$ contributions can dominate at low temperatures and a spin-reorientation transition [21, 48] occurs at 150 K.

For $ErFe_{11}TiH$ and $NdFe_{11}TiH$ the situation is more complex because, in these compounds, the hydrogen induced modifications of the magnetocrystalline anisotropy cannot be explained in terms of the changes in the A_{nm} parameters reported [23] for $HoFe_{11}Ti$. In $ErFe_{11}Ti$ the spin-reorientation transition is driven by the sixth-order term, which is exceptionally large in this compound. After hydrogenation $B_{60}\langle O_{60}\rangle$ is significantly reduced, whereas the axial $B_{20}\langle O_{20}\rangle$ contribution becomes more negative, see table 2. Consequently, in $ErFe_{11}TiH$ a significant increase in the axial contribution of erbium to the total anisotropy would be expected. In contrast, only a small decrease in the spin-reorientation temperature, from 50 K in $ErFe_{11}Ti$ to 40 K in $ErFe_{11}TiH$, is observed. The spin reorientations in $ErFe_{11}Ti$ and $ErFe_{11}TiH$ were investigated by several authors [3, 4, 47] and there is no agreement on their order or smoothness. The sharp peak in χ_{ac} at 50 K for $ErFe_{11}Ti$ seems to be characteristic [49] of a first-order transition from an axial to a canted magnetic phase, whereas the step-like anomaly in χ_{ac} for $ErFe_{11}TiH$ seems to be characteristic of a second-order transition in which the canting angle continuously changes with temperature. The completely different temperature dependence of χ_{ac} for $ErFe_{11}Ti$ and $ErFe_{11}TiH$ may indicate that the spin-reorientation transitions are of a different order and further measurements are necessary to confirm the order of these transitions.

In going from $NdFe_{11}Ti$ to $NdFe_{11}TiH$, the spin-reorientation temperature decreases from 200 to 125 K. The temperature dependence of χ_{ac} is very similar in both $NdFe_{11}Ti$ and $NdFe_{11}TiH$, exhibiting a sharp peak at the transition temperature and indicate a first-order transition. Mössbauer spectra [15] provide more information about the canted magnetic phase. The nearly zero average quadrupole shift observed [15] in the iron-57 Mössbauer spectra of $NdFe_{11}Ti$ below 200 K indicates a canted magnetic phase with a canting angle close to 54.7°, a value that is in good agreement with the 60° value reported by Hu *et al* [28]. In a similar fashion, the average quadrupole shift of about -0.07 mm s^{-1} observed [15] in $NdFe_{11}TiH$ below 125 K indicates a canting angle of between 60° and 90° or even a basal magnetic phase. Similarly, in $NdFe_{10.5}Mo_{0.5}$ [50], after hydrogenation, the transition temperature decreases whereas the canting angle from the c-axis increases. In $NdFe_{11}Ti$ the spin-reorientation transition is driven by the second-order and fourth-order crystal field terms, terms which give a basal contribution to the total magnetic anisotropy. After hydrogenation the basal $B_{20}\langle O_{20}\rangle$ contribution is greatly enhanced, whereas the axial $B_{60}\langle O_{60}\rangle$ contribution is much less negative, see table 2. Consequently, a reinforcement of the neodymium basal contribution to the magnetocrystalline anisotropy and an increase in transition temperature would be expected in disagreement with experimental observation. In other words, although the variation of the A_{nm} parameters obtained for $HoFe_{11}TiH$ correctly predicts the stable magnetic phase at zero kelvin, it cannot explain the observed decrease in the spin-reorientation temperature upon hydrogenation. Consequently, at least for $NdFe_{11}Ti$ and $ErFe_{11}Ti$ and their hydrides, a more detailed analysis of the different contributions to the magnetocrystalline anisotropy is necessary.

3. Temperature dependence of the anisotropy and the spin-reorientation transitions

The temperature dependence of the rare-earth contribution to the magnetocrystalline anisotropy can be calculated in a linear approximation of the crystal field, an approximation which is taken to be a perturbation of the strong 3d–4f exchange interaction. In this section, the model proposed by Kuz'min [49, 51] is applied to the $RFe_{11}Ti$ and $RFe_{11}TiH$ compounds. This model permits a calculation of the temperature dependence of the rare-earth phenomenological anisotropy coefficients in terms of the generalized Brillouin functions, as follows,

$$K_{1R} = -3J^2B_{20}B_J^2(x) - 40J^4B_{40}B_J^4(x) - 168J^6B_{60}B_J^6(x), \tag{5a}$$

$$K_{2R} = 35J^4B_{40}B_J^4(x) + 378J^6B_{60}B_J^6(x), \tag{5b}$$

$$K_{3R} = -231J^6B_{60}B_J^6(x), \tag{5c}$$

$$K'_{2R} = J^4B_{44}B_J^4(x) + 10J^6B_{64}B_J^6(x) \tag{5d}$$

and

$$K'_{3R} = -11J^6B_{64}B_J^6(x), \tag{5e}$$

where x is $2J(g_J - 1)\mu_B B_{ex}/kT$ and $B_J^n(x)$ are the generalized Brillouin functions defined by Kuz'min [51]. They are expressed in terms of elementary functions by

$$B_J^n(x) = P_n(\xi, \eta) - Q_n(\xi, \eta)\coth[((2J + 1)/2J)x],$$

where $\xi = (1/2J)\coth(x/2J)$, and $\eta = 1/2J$, and P_n (ξ, η) and Q_n (ξ, η) are nth-order polynomials in ξ and η. The polynomials for $n = 2$, 4 and 6 are explicitly given in table I of [51]. The anisotropy energy can then be written as

$$F_a = K_1 \sin^2\theta + [K_2 + K'_2\cos 4\phi]\sin^4\theta + [K_3 + K'_3\cos 4\phi]\sin^6\theta. \tag{6}$$

Table 4. The A_j, B_j and C_j coefficients that give the temperature dependences of K_{1Fe} and K_{2Fe} for the $RFe_{11}Ti$ and $RFe_{11}TiH$ compounds.

Compound	A_1	B_1	C_1	A_2	B_2	C_2
$PrFe_{11}Ti$	−0.10	1.51	−0.39	−0.78	3.03	−1.23
$PrFe_{11}TiH$	−0.17	1.63	−0.45	−0.98	2.10	−0.08
$NdFe_{11}Ti$	−0.11	1.52	−0.40	−0.81	3.07	−1.25
$NdFe_{11}TiH$	−0.20	1.67	−0.46	−1.01	2.13	−0.09
$TbFe_{11}Ti$	−0.19	1.64	−0.44	−0.96	3.35	−1.38
$TbFe_{11}TiH$	−0.22	1.70	−0.47	−1.03	2.16	−0.09
$DyFe_{11}Ti$	−0.11	1.53	−0.40	−0.81	3.08	−1.26
$DyFe_{11}TiH$	−0.16	1.62	−0.44	−0.96	2.08	−0.083
$HoFe_{11}Ti$	−0.061	1.45	−0.37	−0.71	2.89	−1.17
$HoFe_{11}TiH$	−0.13	1.57	−0.43	−0.93	2.05	−0.081
$ErFe_{11}Ti$	−0.02	1.39	−0.35	−0.63	2.74	−1.11
$ErFe_{11}TiH$	−0.09	1.51	−0.40	−0.61	1.39	−0.25

The easy magnetization direction coincides with the [001] direction or remains in the (110) or $(1\bar{1}0)$ planes, so that the angle ϕ is equal to $\pi/4 + n\pi/2$, where $n = 1, 2, 3$ and 4, correspond to four possible domains. Therefore, for some applications, equation (6) can be rewritten as

$$F_a = K_1 \sin^2\theta + [K_2 - K_2'] \sin^4\theta + [K_3 - K_3'] \sin^6\theta. \tag{7}$$

The anisotropy coefficients entering into equation (7) consist of two parts, contributed by the iron and the rare-earth sublattices and can be written as

$$K_j = K_{j\mathrm{Fe}} + K_{j\mathrm{R}}. \tag{8}$$

The iron sublattice contribution to K_1 and K_2 are interpolated [51] as

$$K_{j\mathrm{Fe}}(T) = K_{j\mathrm{Fe}}(0)(A_j + B_j t + C_j t^2) \tag{9}$$

where $t = 1 - T/T_c$ and, for the $RFe_{11}Ti$ compounds, $K_{1Fe}(0) = 24.0$ K/f.u. and $K_{2Fe}(0) = 0.44$ K/f.u., the values obtained [27] for $YFe_{11}Ti$ and for the $RFe_{11}TiH$ compounds, $K_{1Fe}(0) = 25.8$ K/f.u. and $K_{2Fe}(0) = 0.24$ K/f.u., the values obtained [42] for $YFe_{11}TiH$. The A_j, B_j and C_j, $j = 1$ and 2, coefficients must be determined for each compound as noted in [51], and are presented in table 4.

The necessary condition [51] for a spontaneous spin-reorientation transition from an axial to a canted magnetic phase is

$$K_1(T) = K_{1\mathrm{R}}(T) + K_{1\mathrm{Fe}}(T) = 0, \tag{10}$$

and for a spin-reorientation transition from an axial or conical to a basal magnetic phase is

$$K_{\mathrm{eff}}(T) = K_1(T) + K_2(T) + K_3(T) = K_{1\mathrm{R}}(T) + K_{1\mathrm{Fe}}(T) + (K_{2\mathrm{R}}(T) - K_{2\mathrm{R}}'(T)) + K_{2\mathrm{Fe}}(T) + (K_{3\mathrm{R}}(T) - K_{3\mathrm{R}}'(T)) = 0. \tag{11}$$

3.1. Application to the $RFe_{11}Ti$ and $RFe_{11}TiH$ compounds

We begin our analysis of the temperature dependence of the rare-earth contribution to the magnetocrystalline anisotropy with the A_{nm} parameters that correctly reproduce the stable magnetic phase at zero kelvin. An exchange interaction [4, 27], $\mu_B B_{ex}$, of 300 K when R is Nd and Pr, of 126 K when R is Tb, of 121 K when R is Dy, and of 100 K when R is Ho and Er has been used. The temperature dependences of the iron sublattice anisotropy constants, K_{1Fe} and K_{2Fe}, are given by equation (9) with the coefficients given in table 4.

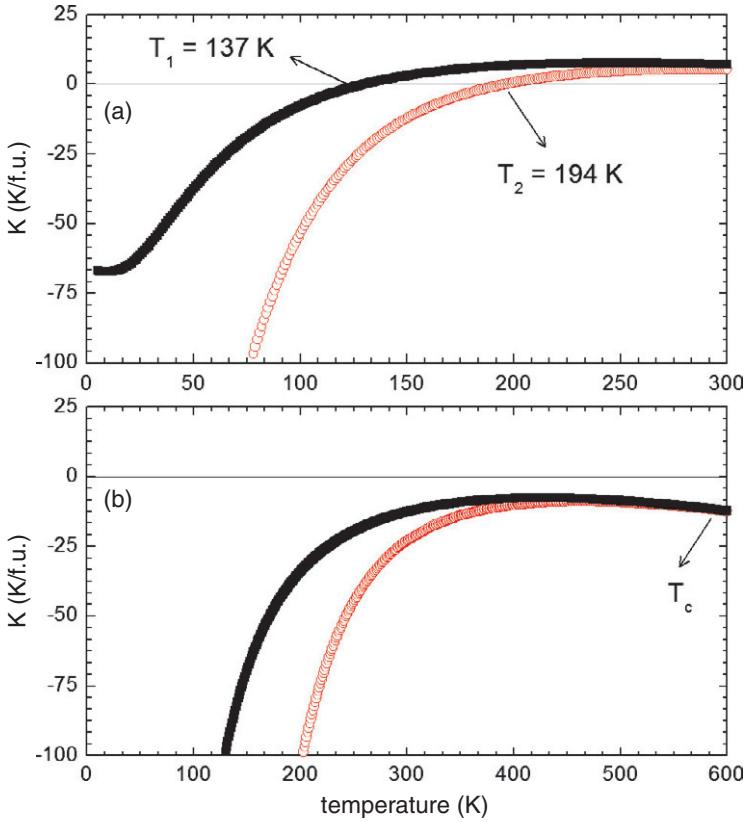

Figure 2. The temperature dependences of $K_1 = K_{1R} + K_{1Fe}$, open circles, and K_{eff}, solid squares, for $DyFe_{11}Ti$, top, and $DyFe_{11}TiH$, bottom. The A_{nm} coefficients for $DyFe_{11}Ti$ and $DyFe_{11}TiH$ have been obtained from [27] and [23], respectively.

We have found that the A_{nm} parameters that correctly reproduce the stable magnetic phase at zero kelvin also reproduce the magnetic behaviour as a function of the temperature only when R is Dy, Ho and Tb. The temperature dependences of K_1 and K_{eff} as defined in equations (10) and (11) are shown in figures 2–4, when R is Dy, Ho and Tb, respectively. For $DyFe_{11}Ti$ the model predicts a first spin-reorientation transition at 194 K from axial to canted and a second spin-reorientation transition at 137 K from canted to basal, predictions that are in reasonable agreement with experimental results [4, 13, 23, 44]. Furthermore, the model correctly predicts that $DyFe_{11}TiH$ adopts a basal magnetic phase at all temperatures below its Curie temperature of 600 K [8]. For $HoFe_{11}Ti$ the model predicts that the compound is axial between 4.2 K and its Curie temperature of 553 K, see figure 3, in agreement with the experimental results [4, 11, 21, 28, 48, 52]. For $HoFe_{11}TiH$, the model predicts a spin-reorientation transition from an axial to a canted magnetic phase at 105 K, a temperature somewhat smaller than the experimental value of 150 K [11, 48]. For $TbFe_{11}Ti$ both K_1 and K_{eff} are zero at 250 K, figure 4, indicating that a spin-reorientation transition from an axial to a basal magnetic phase occurs at this temperature, in reasonable agreement with the experimentally observed transition at 330 K [4, 14, 25, 41, 53]. Furthermore, the A_{nm} parameters reported for $TbFe_{11}TiH$ correctly predict [8, 14, 25] that this compound adopts a basal magnetic phase between 4.2 K and its Curie temperature of 620 K.

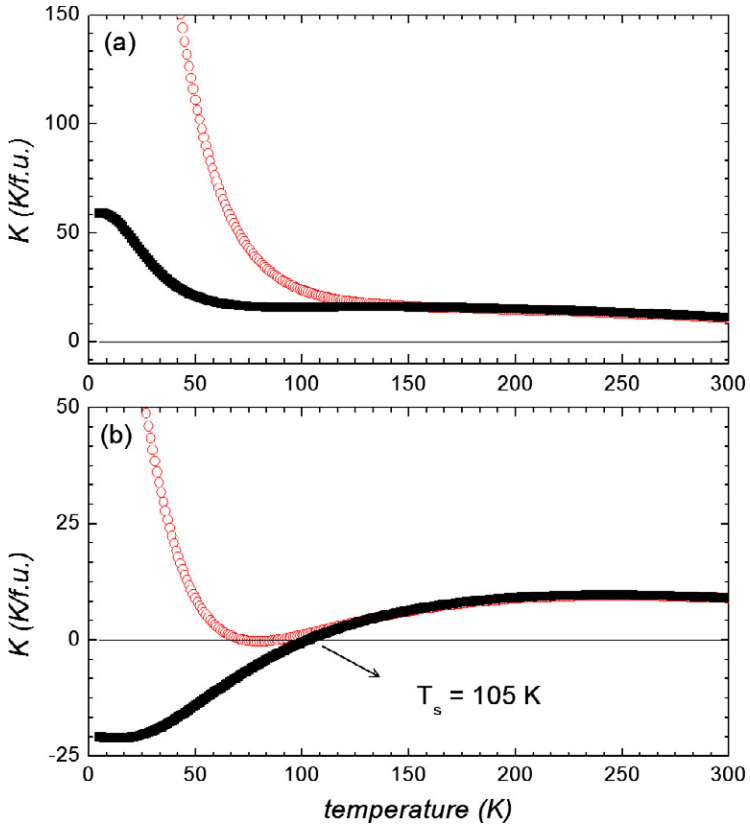

Figure 3. The temperature dependences of $K_1 = K_{1R} + K_{1Fe}$, open circles, and K_{eff}, solid squares, for $HoFe_{11}Ti$, top, and $HoFe_{11}TiH$, bottom. The A_{nm} coefficients for $HoFe_{11}Ti$ and $HoFe_{11}TiH$ have been obtained from [27] and [23], respectively.

For the rest of the compounds, the A_{nm} parameters that correctly reproduce the stable magnetic phase at zero kelvin do not reproduce the magnetic behaviour as a function of the temperature. This result is not unexpected for $ErFe_{11}TiH$ and $NdFe_{11}TiH$, as we have discussed in section 2.2. Surprisingly, the A_{nm} parameters that correctly reproduce the stable magnetic phase at zero kelvin for $ErFe_{11}Ti$ and $PrFe_{11}Ti$ do not reproduce the temperature dependence of the magnetic behaviour.

3.1.1. $ErFe_{11}Ti$ and $ErFe_{11}TiH$. The temperature dependences of K_1 and K_{eff} obtained with the A_{nm} parameters that correctly predict the stable magnetic phase of $ErFe_{11}Ti$ and $ErFe_{11}TiH$ at zero kelvin are shown in the insets in figure 5. For $ErFe_{11}Ti$, see the inset to figure 5(a), the model predicts a spin-reorientation transition from an axial to a canted magnetic phase at 55 K, a prediction that is in excellent agreement with the experimentally observed [4, 10, 28, 54] transition at 50 K. Unfortunately, these parameters also predict a further spin reorientation from a canted to a basal phase at 30 K, a transition that is not experimentally observed.

The experimentally observed spin-reorientation transition in $ErFe_{11}Ti$ at 50 K is driven by the sixth-order crystal field term, $B_{60}\langle O_{60}\rangle$. Consequently, the prediction of two spin-reorientation transitions by our model probably indicates that the A_{60} parameter reported for $HoFe_{11}Ti$ is greater than the actual A_{60} parameter of $ErFe_{11}Ti$. Indeed, the A_{nm} parameters

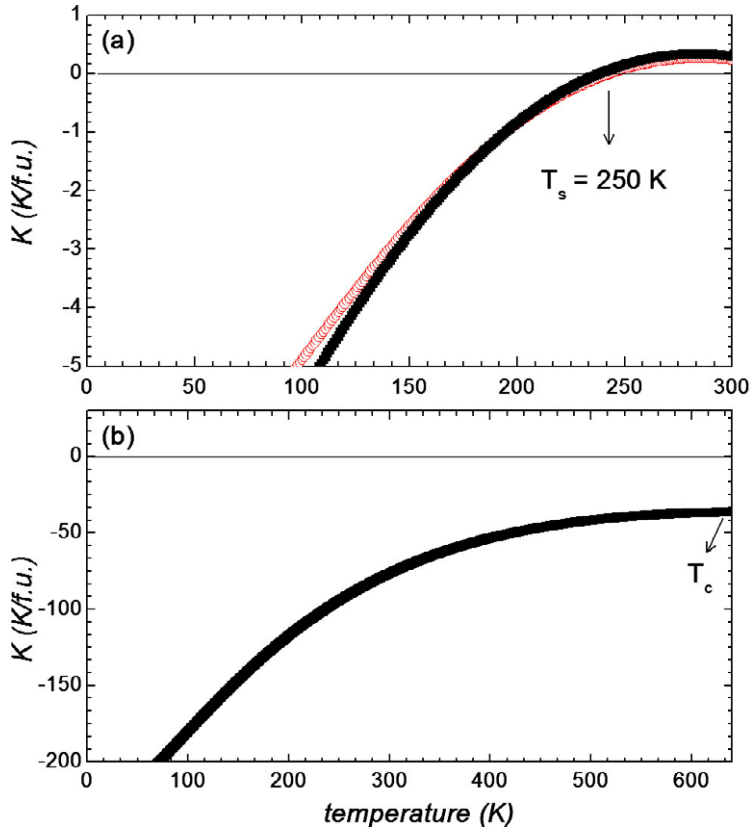

Figure 4. The temperature dependences of $K_1 = K_{1R} + K_{1Fe}$, open circles, and K_{eff}, solid squares, for $TbFe_{11}Ti$, top, and $TbFe_{11}TiH$, bottom. The A_{nm} coefficients for $TbFe_{11}Ti$ have been obtained from [27]. The A_{nm} parameters for $TbFe_{11}TiH$ have been obtained by assuming that the A_{nm} coefficients of $TbFe_{11}Ti$ vary upon hydrogenation as is proposed in [23].

reported by Kou *et al* [4] from magnetic measurements on polycrystalline $ErFe_{11}Ti$, i.e., $A_{20} = -21.8\ \mathrm{K}a_0^{-2}$, $A_{40} = -3.0\ \mathrm{K}a_0^{-4}$, $A_{60} = 1.5\ \mathrm{K}a_0^{-6}$, $A_{44} = 70.9\ \mathrm{K}a_0^{-4}$ and $A_{64} = 0\ \mathrm{K}a_0^{-6}$, correctly predict just one spin-reorientation transition at about 45 K from an axial to a canted magnetic phase, see figure 5(a). The main difference between the predictions from the parameters of Abadia *et al* [27] and of Kou *et al* [4] results from the value of the $B_{60}\langle O_{60}\rangle$ term; Kou *et al* [4] have reported an A_{60} parameter which is five times smaller than that reported by Abadia *et al* [27]. Consequently, with the parameters reported by Kou *et al* [4] the planar contribution to the net rare-earth anisotropy is reduced and just one spin reorientation is predicted, in agreement with the experimental results.

The A_{nm} parameters obtained for $HoFe_{11}TiH$ [23] do not predict the experimentally observed [10, 54] spin reorientation at 40 K in $ErFe_{11}TiH$, as is shown in the inset in figure 5(b). Very similar results are obtained for $ErFe_{11}TiH$ if the A_{nm} parameters reported by Kou *et al* [4] are used and assumed to vary by the same relative amount upon hydrogenation as in the $HoFe_{11}TiH$ case. This result is not unexpected because, as is explained above, in $ErFe_{11}Ti$ the spin-reorientation transition is driven by the sixth-order term. After hydrogenation $B_{60}\langle O_{60}\rangle$ is significantly reduced and the axial $B_{20}\langle O_{20}\rangle$ contribution is increased, see table 2. Hence, if the variation of the A_{nm} parameters reported for $HoFe_{11}TiH$ is used, a significant increase

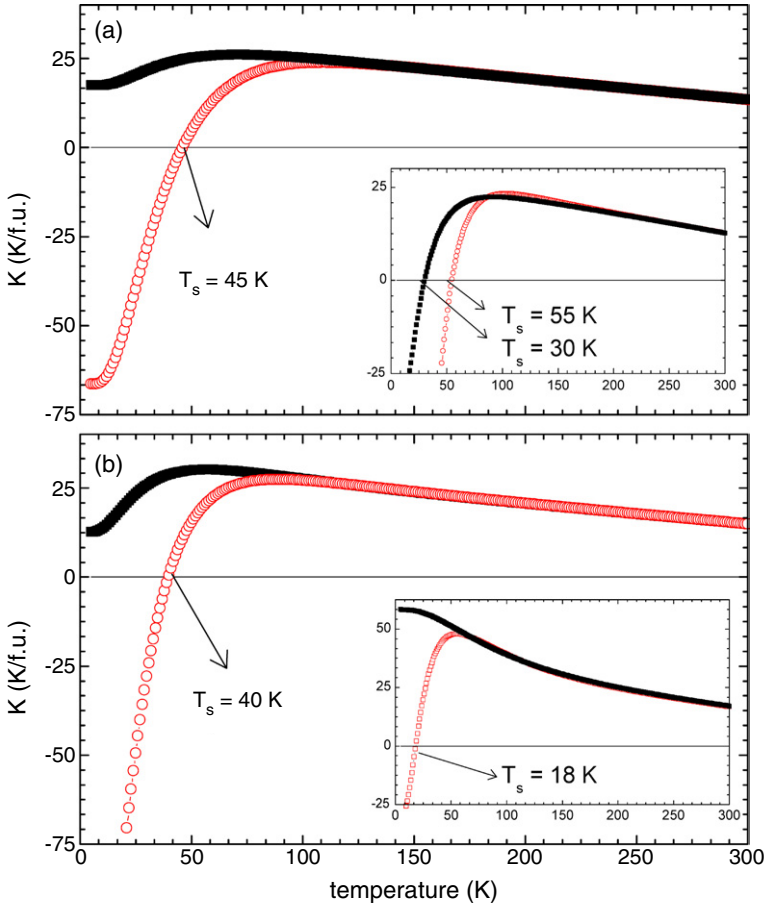

Figure 5. The temperature dependences of $K_1 = K_{1R} + K_{1Fe}$, open circles, and K_{eff}, solid squares, for $ErFe_{11}Ti$, (a), and $ErFe_{11}TiH$. (b) The A_{nm} coefficients for $ErFe_{11}Ti$ were obtained from [4] and $A_{20} = -43.7$ Ka_0^{-2} was used for $ErFe_{11}TiH$. Insets: the temperature dependences of $K_1 = K_{1R} + K_{1Fe}$, open circles, and K_{eff}, solid squares, for $ErFe_{11}Ti$, (a) and $ErFe_{11}TiH$, (b), predicted by the A_{nm} coefficients reported in [27] and [23], respectively.

in the axial contribution of the erbium to the total anisotropy is expected. In fact, these parameters predict a spin reorientation at 18 K, as is shown in the inset in figure 5(b). It should be noted that the A_{nm} parameters obtained for $HoFe_{11}TiH$ give the correct trend for the spin-reorientation temperature, i.e., the spin-reorientation temperature decreases upon hydrogenation, but the predicted 18 K is lower than the experimentally observed 40 K. This result suggests that the relative variations Δ_{nm} of the A_{nm} parameters upon hydrogenation of $ErFe_{11}Ti$ are smaller. Hence, Δ_{nm} values that are smaller than those reported for $HoFe_{11}Ti$ have been tried to reproduce the experimentally observed spin-reorientation temperature in $ErFe_{11}TiH$. In this way, the A_{nm} parameters reported in table 5 have been obtained. These parameters, which approximately correspond to relative variations in Δ_{nm} that are five times smaller than those obtained for $HoFe_{11}TiH$, predict a slight decrease of the spin-reorientation temperature from 45 to 40 K, a prediction that is in agreement with the experimental results. The temperature dependences of K_1 and K_{eff} obtained with these parameters are shown in figure 5(b). Although these A_{nm} parameters for $ErFe_{11}TiH$ should be refined with the fit of

Table 5. The A_{nm} parameters, in $K a_0^{-n}$, that reproduce the magnetic properties of the $RFe_{11}Ti$ and $RFe_{11}TiH$ compounds.

Compound	A_{20}	A_{40}	A_{60}	A_{44}	A_{64}
$PrFe_{11}Ti$	−58.7	−11.1	5.02	−153.2	−0.81
$PrFe_{11}TiH$	−337.5	−8.5	1.40	−200.0	−0.85
$NdFe_{11}Ti$	−40.4	−6.9	0.30	36.6	0
$NdFe_{11}TiH$	−76.8	−6.9	0.30	36.6	0
$SmFe_{11}Ti$	−20.5	−11.1	5.02	−153.2	−0.81
$SmFe_{11}TiH$	−118	−8.5	1.40	−200.0	−0.85
$TbFe_{11}Ti$	−52.5	−0.27	0.021	−0.0087	−8.9
$TbFe_{11}TiH$	−302.3	−0.21	0.006	−0.011	−9.3
$DyFe_{11}Ti$	−20.5	−11.1	5.02	−153.2	−0.81
$DyFe_{11}TiH$	−118	−8.5	1.40	−200.0	−0.85
$HoFe_{11}Ti$	−20.5	−11.1	5.02	−153.2	−0.81
$HoFe_{11}TiH$	−118	−8.5	1.40	−200.0	−0.85
$ErFe_{11}Ti$	−21.8	−3.0	1.50	70.9	0
$ErFe_{11}TiH$	−43.7	−3.0	1.50	70.9	0

other experimental points, some general trends are clear, i.e., the A_{20} parameter becomes more negative upon hydrogenation and there is virtually no relative variations of the remaining A_{nm} parameters.

3.1.2. $NdFe_{11}Ti$ and $NdFe_{11}TiH$. The temperature dependences of K_1 and K_{eff} obtained with the A_{nm} parameters [23] that correctly predict the stable magnetic phase at zero kelvin are shown in figure 6(a) and the inset in figure 6(b). For $NdFe_{11}Ti$, see figure 6(a), K_1 is zero at 195 K, in good agreement with the observed [15] spin reorientation from an axial to a canted magnetic phase at 200 K. In contrast, for $NdFe_{11}TiH$, see inset in figure 6(b), these A_{nm} parameters [23] predict a basal magnetic phase below its Curie temperature of 614 K. This result is not unexpected as has been explained in section 2.2. In $NdFe_{11}Ti$, the spin-reorientation transition is driven by the second-order and fourth-order crystal field terms, terms that yield basal contributions to the total anisotropy. After hydrogenation, the basal $B_{20}\langle O_{20}\rangle$ contribution is greatly enhanced, whereas the axial $B_{60}\langle O_{60}\rangle$ contribution is reduced, see table 2. Consequently, a reinforcement of the neodymium basal contribution to the magnetocrystalline anisotropy and an increase in the spin-reorientation temperature would be expected. However, a decrease in the spin-reorientation temperature is experimentally observed. It should be noted that this surprising behaviour of $NdFe_{11}TiH$ is very different from that observed in $ErFe_{11}TiH$. In the case of neodymium, the Δ_{nm} relative variations reported for $HoFe_{11}TiH$ predict a change in the magnetocrystalline anisotropic properties that is the *opposite* of the experimentally observed change. The origin of this discrepancy is not clear. It is possible that, as it is the case for erbium, the Δ_{nm} relative variations are smaller than those found for the hydrogenation of $HoFe_{11}Ti$, or that the Δ_{nm} relative variations are different for light rare earths.

We have explored the first possibility and assumed that the Δ_{nm} relative variations are smaller than those found for $HoFe_{11}Ti$. By trying different sets of Δ_{nm} coefficients, the A_{nm} parameters given in table 5 were found to best reproduce the experimentally observed magnetic behaviour of $NdFe_{11}TiH$. It should be noted that values of A_{20} smaller than those reported in table 5 predict the appearance of two spin-reorientation transitions. As is the case for $ErFe_{11}TiH$, these parameters correspond to negligible relative variations, Δ_{nm}. However, for

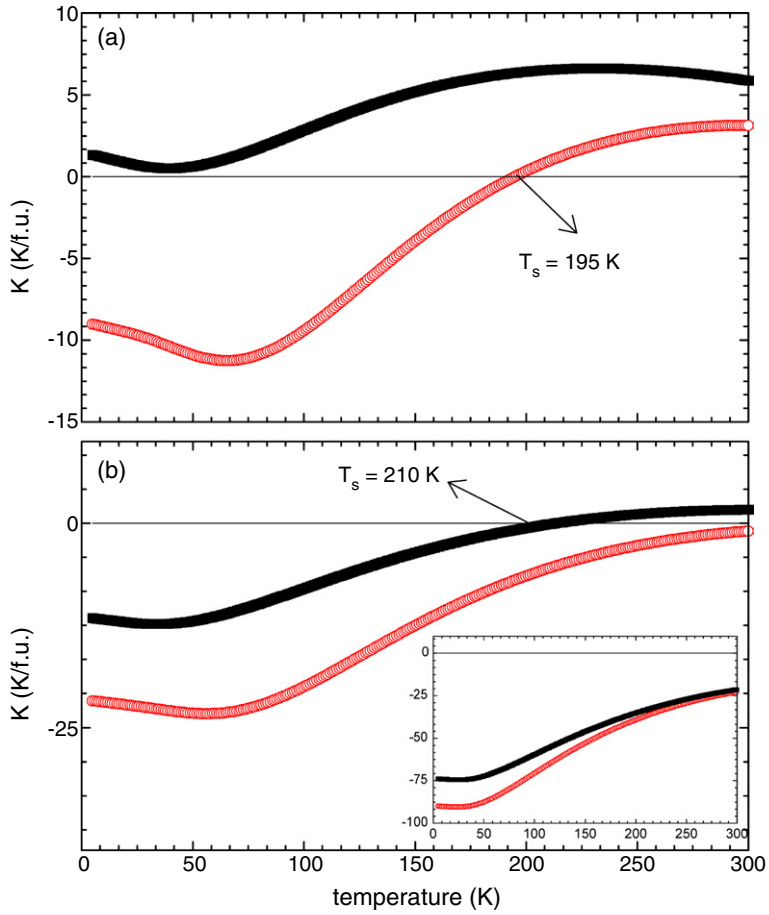

Figure 6. The temperature dependences of $K_1 = K_{1R} + K_{1Fe}$, open circles, and K_{eff}, solid squares, for $NdFe_{11}Ti$, (a), and $NdFe_{11}TiH$. (b) The A_{nm} coefficients for $NdFe_{11}Ti$ were obtained from [27] and $A_{20} = -83.8$ Ka_0^{-2} was used for $NdFe_{11}TiH$. Inset: the temperature dependences of $K_1 = K_{1R} + K_{1Fe}$, open circles, and K_{eff}, solid squares, for $NdFe_{11}TiH$ predicted by the A_{nm} coefficients reported in [23].

$NdFe_{11}TiH$ the agreement is not very good; the predicted spin-reorientation transition from an axial to a basal phase takes place at 210 K, a temperature that is significantly higher than the experimental [15] 125 K, see figure 6(b). In other words, the model does not reproduce the decrease in spin-reorientation temperature that takes place upon hydrogenation of $NdFe_{11}Ti$. This disagreement clearly indicates that in $NdFe_{11}Ti$ the A_{nm} parameters behave differently upon hydrogenation than in the remaining $RFe_{11}Ti$ compounds, and very probably that the use of the A_{nm} parameters obtained for the heavy rare-earth compounds with the light rare-earth compounds is an oversimplification. The decrease in spin-reorientation temperature suggests an increase of A_{60} upon hydrogenation because, in the case of neodymium, the axial contribution originates from the $B_{60}\langle O_{60}\rangle$ term. Unfortunately, it is not possible to obtain a reliable set of A_{nm} parameters from the fit of only one experimental point, i.e., the spin-reorientation temperature. A more detailed analysis, such as the fit of the magnetization versus field, is necessary for $NdFe_{11}TiH$.

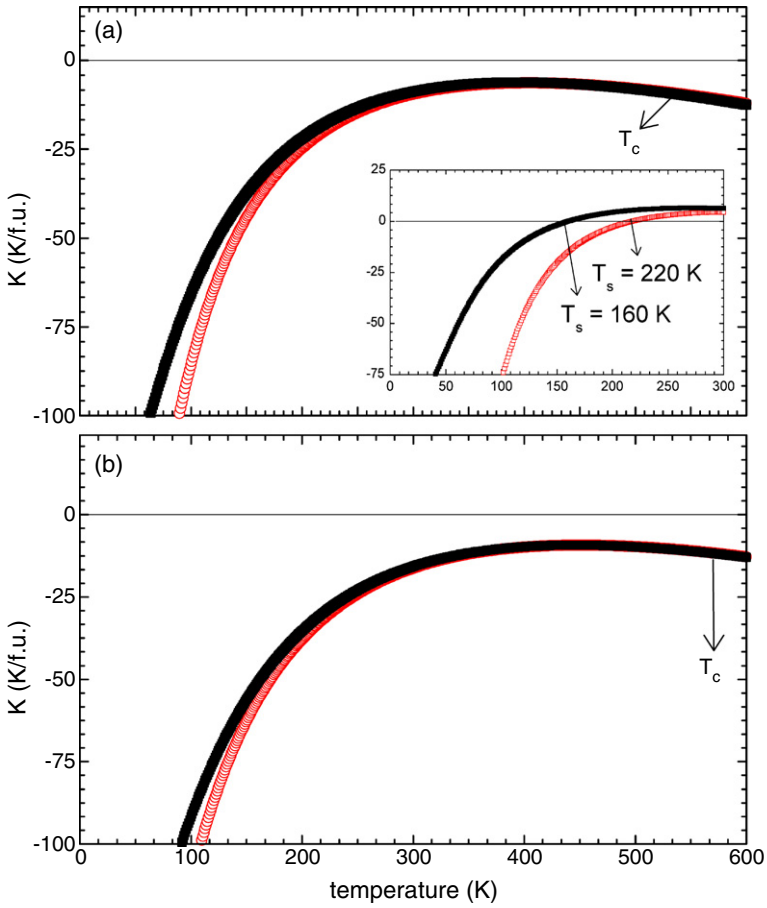

Figure 7. The temperature dependences of $K_1 = K_{1R} + K_{1Fe}$, open circles, and K_{eff}, solid squares, for $PrFe_{11}Ti$, (a), and $PrFe_{11}TiH$, (b). The A_{nm} coefficients for $PrFe_{11}Ti$ were obtained from [27] but with a more negative A_{20} parameter of -58.7 Ka_0^{-2}. The A_{nm} parameters for $PrFe_{11}TiH$ have been obtained by assuming that the A_{nm} coefficients of $PrFe_{11}Ti$ vary upon hydrogenation as reported in [23]. Inset: the temperature dependences of $K_1 = K_{1R} + K_{1Fe}$, open circles, and K_{eff}, solid squares, for $PrFe_{11}Ti$ predicted by the A_{nm} coefficients reported in [27].

3.1.3. $PrFe_{11}Ti$ and $PrFe_{11}TiH$. The temperature dependences of K_1 and K_{eff} obtained with the A_{nm} parameters [27] that correctly predict the stable magnetic phase at zero kelvin of $PrFe_{11}Ti$ are shown in the inset in figure 7(a). As may be observed in this figure, these parameters do not reproduce the experimentally observed magnetic behaviour of $PrFe_{11}Ti$. The parameters correctly predict that the compound adopts a basal magnetic phase at zero kelvin, but they also predict two spin-reorientation transitions at 160 and 220 K, transitions that are not experimentally observed. This wrong prediction supports our hypothesis about the inadequacy of the A_{nm} parameters obtained for the heavy rare earths for the light rare earths.

We tried to reproduce the experimentally observed magnetic behaviour of $PrFe_{11}Ti$ by using a more negative value of A_{20}, the term that is mainly responsible for the planar magnetic anisotropy. We found that a value of A_{20} of -58.7 Ka_0^{-2}, is required to predict that $PrFe_{11}Ti$ is planar from 4.2 K up to its Curie temperature. Such a value is in excellent agreement with the value of $-50(10)$ Ka_0^{-2} obtained for $GdFe_{11}Ti$ [20]. By assuming that A_{20}

varies upon hydrogenation as in $HoFe_{11}Ti$, i.e., $A_{20}(x) = A_{20}(0) + 4.75\ A_{20}(0)$, we obtain $A_{20} = -337.5\ \mathrm{K}a_0^{-2}$ for $PrFe_{11}TiH$. The corresponding temperature dependences of K_1 and K_{eff} for $PrFe_{11}Ti$ and $PrFe_{11}TiH$ are shown in figures 7(a) and (b), respectively.

4. Conclusions

The final A_{nm} parameters that reproduce the magnetic phase diagrams of the $RFe_{11}Ti$ and $RFe_{11}TiH$ compounds are given in table 5. For the $RFe_{11}Ti$ compounds where R is Tb, Dy and Ho, the A_{nm} parameters obtained from the fit of the single-crystal magnetization curves [27, 28] correctly predict the temperature dependence of the macroscopic magnetocrystalline anisotropy.

For the remaining compounds where R is Pr, Nd and Er, for which there are no reports of A_{nm} parameters resulting from the fit of single-crystal magnetization curves, we have found that the A_{nm} parameters reported for R = Ho or Dy, are unable to reproduce the temperature dependence of the magnetocrystalline anisotropy. For these compounds, we have used the model proposed by Kuz'min [49, 51] to determine the A_{nm} parameters that best reproduce their magnetocrystalline anisotropy.

For $PrFe_{11}Ti$ a more negative A_{20} value than that reported earlier [27, 28] is required to reproduce its basal magnetic phase from 4.2 K to the Curie temperature. This more negative value is in perfect agreement with the value measured [20] by gadolinium-155 Mössbauer spectral studies of $GdFe_{11}Ti$. For $NdFe_{11}Ti$ and $ErFe_{11}Ti$ the A_{nm} parameters reported earlier [27, 28] cannot predict the spin-reorientation transitions that occur in these compounds. However, these spin-reorientation transitions can be reproduced with the A_{nm} parameters reported by Kou *et al* [4] from magnetic measurements on polycrystalline samples.

Thus, for the $RFe_{11}Ti$ compounds, different A_{20} values have been used to reproduce their magnetic anisotropy and its temperature dependence. Variations in A_{20} values with the rare earth are not unexpected, as A_{20} measures the electric field gradient at the rare-earth site, a gradient that depends directly on the charge distribution. The charge distribution itself is very sensitive to the lattice parameters. In the $RFe_{11}Ti$ compounds, an anisotropic lattice contraction is observed throughout the rare-earth series and is reflected, in a complex fashion, in the different A_{20} values.

For the $RFe_{11}TiH$ compounds, the variation upon hydrogenation of the crystal field parameters reported for $HoFe_{11}TiH$ [23] correctly describes the magnetic behaviour when R is Tb, Dy, Ho and Pr. However, these parameters predict a significant reduction in the basal contribution of the erbium sublattice to the total magnetocrystalline anisotropy, a reduction that is not experimentally observed. The spin-reorientation transition experimentally observed in $ErFe_{11}TiH$ can be reproduced by assuming that the relative variations of the A_{nm} parameters upon hydrogenation are smaller in $ErFe_{11}Ti$ than in $HoFe_{11}Ti$.

For $NdFe_{11}TiH$, the variation upon hydrogenation of the A_{nm} parameters reported for $HoFe_{11}TiH$ predicts a significant increase in the basal contribution of the neodymium sublattice to the total magnetocrystalline anisotropy, an increase that is not experimentally observed. As in $ErFe_{11}TiH$, the spin reorientation that occurs in $NdFe_{11}TiH$ may be reproduced by assuming that the relative variations in the A_{nm} parameters upon hydrogenation are smaller than in $HoFe_{11}Ti$. However, it is not possible to reproduce the experimentally observed decrease in spin-reorientation temperature that takes place upon hydrogenation.

Throughout the $RFe_{11}TiH$ series, the main influence of hydrogen is to modify A_{20}. This modification is again expected [20] because hydrogen is the nearest neighbour of the rare earth, introduces a lattice expansion and modifies the charge distribution around the rare earth.

Similar effects resulting from the insertion of hydrogen, carbon and nitrogen into rare-earth–iron intermetallic compounds have been described earlier [55, 56].

In conclusion, the magnetic anisotropy and its temperature dependence in the $RFe_{11}TiH$ and $RFe_{11}TiH$ compounds result mainly from the rare-earth contribution; the iron contribution to the anisotropy does not vary [22] much either with the rare earth or upon hydrogenation. The first-order crystal field term makes a major contribution and in some cases is found to be more negative than had previously been reported. However, the higher-order terms cannot be ignored [57] in describing the magnetic properties of the $RFe_{11}Ti$ and $RFe_{11}TiH$ compounds.

Acknowledgments

The financial support of the University of Liège for grant number 2850006 and of the 'Fonds de la Recherche Fondamentale Collective' for grant 2.4522.01 is acknowledged with thanks. This work was partially supported by the US National Science Foundation through grants DMR95-21739 and INT-9815138, the Ministère de la Communauté Française de Belgique, convention PVB/ADK/FR/ad2685 and the 'Centre National de la Recherche Scientifique, France' through grants action initiative numbers 7418 and 18213.

References

[1] de Mooij D B and Buschow K H J 1988 *J. Less Common Met.* **136** 207
[2] Buschow K H J 1991 *J. Magn. Magn. Mater.* **100** 79
[3] Hu B P, Li H S, Gavigan J P and Coey J M D 1989 *J. Phys.: Condens. Matter* **1** 755
[4] Kou X C, Zhao T S, Grössinger R, Kirchmayer H R, Li X and de Boer F R 1993 *Phys. Rev.* B **47** 3231
[5] Kuz'min M D and Zvezdin A K 1998 *J. Appl. Phys.* **83** 3239
[6] Zhang L Y and Wallace W E 1989 *J. Less-Common Met.* **149** 371
[7] Nikitin S A, Tereshina I S, Verbetsky V N and Salamova A A 2001 *J. Alloys Compounds* **316** 46
[8] Isnard O 2003 *J. Alloys Compounds* **356/357** 17
[9] Long G J, Hautot D, Grandjean F, Isnard O and Miraglia S 1999 *J. Magn. Magn. Mater.* **202** 100
[10] Piquer C, Hermann R P, Grandjean F, Long G J and Isnard O 2003 *J. Appl. Phys.* **93** 3414
[11] Piquer C, Grandjean F, Long G J and Isnard O 2003 *J. Alloys Compounds* **353** 33–4
[12] Piquer C, Isnard O, Grandjean F and Long G J 2003 *J. Magn. Magn. Mater.* **263** 235–42
[13] Piquer C, Isnard O, Grandjean F and Long G J 2003 *J. Magn. Magn. Mater.* **265** 156
[14] Piquer C, Hermann R P, Grandjean F, Isnard O and Long G J 2003 *J. Phys.: Condens. Matter* **15** 7395
[15] Piquer C, Grandjean F, Isnard O, Pop V and Long G J 2004 *J. Appl. Phys.* **95** 6308
[16] Piquer C, Grandjean F, Isnard O, Pop V and Long G J 2004 *J. Alloys Compounds* **277** 1
[17] Piquer C, Grandjean F, Long G J and Isnard O 2005 *J. Alloys Compounds* **388** 6
[18] Piquer C, Grandjean F, Long G J and Isnard O 2006 *J. Phys.: Condens. Matter* **18** 205
[19] Isnard O, Guillot M, Miraglia S and Fruchart D 1996 *J. Appl. Phys.* **79** 5542
[20] Isnard O, Vulliet P, Sanchez J P and Fruchart D 1998 *J. Magn. Magn. Mater.* **189** 47
[21] Apostolov A, Bezdushnyi R, Stanev N, Damianova R, Fruchart D, Isnard O and Soubeyroux J L 1997 *J. Alloys Compounds* **253/254** 318
[22] Isnard O, Miraglia S, Guillot M and Fruchart D 1998 *J. Alloys Compounds* **275–277** 637
[23] Nikitin S A, Tereshina I S, Pankratov N Yu and Skourski Yu V 2001 *Phys. Rev.* B **63** 134420
[24] Isnard O and Guillot M 1998 *J. Appl. Phys.* **83** 6730
[25] Nikitin S A, Tereshina I S, Verbetsky V N, Salamova A A, Skokov K P, Pankratov N Yu, Skourski Yu V, Tristan N V, Zubenko V V and Telegina I V 2001 *J. Alloys Compounds* **322** 42
[26] Tereshina I S, Nikitin S A, Pankratov N Yu, Bezkorovajnaya G A, Salamova A A, Verbetsky V N, Mydlarz T and Skourski Yu V 2001 *J. Magn. Magn. Mater.* **231** 213
[27] Abadia C, Algarabel P A, Garcia-Landa B, Ibarra M R, del Moral A, Kudrevatykh N V and Markin P E 1998 *J. Phys.: Condens. Matter* **10** 349
[28] Hu B P, Sun H, Coey J M D and Gavigan J P 1990 *Phys. Rev.* B **41** 2221
[29] Hu B P, Wang K Y, Wang Y Z, Wang Z X, Yan Q W, Zhang P L and Sun X D 1995 *Phys. Rev.* B **51** 2905
[30] Rudowicz C 1985 *J. Phys. C: Solid State Phys.* **18** 1415

[31] Stevens K W H 1952 *Proc. R. Soc.* A **65** 209
[32] Buschow K H J, de Mooij D B, Brouha M M, Smit H H A and Thiel R C 1988 *IEEE Trans. Magn.* **24** 1161
[33] Dirken M W 1991 *PhD Thesis* Univ. Leiden
[34] Middleton D P, Mulder F M, Thiel R C and Buschow K H J 1995 *J. Magn. Magn. Mater.* **146** 123
[35] Freeman A J and Desclaux J P 1979 *J. Magn. Magn. Mater.* **12** 11
[36] Franse J J M and Radwanski R J 1993 *Handbook of Magnetic Materials* vol 7, ed K H J Buschow (Amsterdam: North-Holland) chapter 5
[37] Yamada M 1998 *Phys. Rev.* B **38** 620
[38] Kuz'min M D 2000 *J. Appl. Phys.* **88** 7217
[39] Guslienko K Yu, Kou X C and Grössinger R 1995 *J. Magn. Magn. Mater.* **150** 383
[40] Luong N H, Thuy N P and Franse J J M 1992 *J. Magn. Magn. Mater.* **104–107** 1301
[41] Kazakov A A, Kudrevatykh N V and Markin P E 1995 *J. Magn. Magn. Mater.* **146** 208
[42] Tereshina I S, Gaczy'nski P, Rusakov V S, Nikitin S A, Suski W, Tristan N V and Palewski T 2001 *J. Phys.: Condens. Matter* **13** 8161
[43] Kaneko T, Yamada M, Ohashi K, Tawara Y, Osugi R, Yoshio H, Kido G and Nakagawa Y 1989 *10th Int. Workshop on Rare-earth Magnets and Their Applications (Kyoto, 1989)*
[44] Apostolov A, Bezdushnyi R, Damianova R, Stanev N and Naumova I 1995 *J. Magn. Magn. Mater.* **150** 393
[45] Arnold Z, Kamaràd J, Mikulina O, Garcia-Landa B and Ibarra M R 2000 *Proc. 11th Int. Symp. on Magnetic Anisotropy and Coercivity in Rare-Earth Transition Metal Alloys* ed H Kaneko, M Homma and M Okada (Tokyo: The Japan Institute of Metals) p S35
[46] Janssen Y, Brück E, Buschow K H J, de Boer F R, Kamaràd J and Kudrevatykh N V 2002 *J. Magn. Magn. Mater.* **242–245** 1064
[47] Andreev A V, Sechovsky V, Kudrevatykh N V, Sigaev S S and Tarasov E N 1988 *J. Less-Common Met.* **144** L21
[48] Apostolov A, Bezdushnyi R, Stanev N, Damianova R, Fruchart D, Soubeyroux J L and Isnard O 1998 *J. Alloys Compounds* **265** 1
[49] Kuz'min M D, Garcia L M, Artigas M and Bartolomé J 1996 *Phys. Rev.* B **54** 4093
[50] Tomey E, Bacmann M, Fruchart D, Soubeyroux J L and Gignoux D 1995 *J. Alloys Compounds* **231** 195
[51] Kuz'min M D 1992 *Phys. Rev.* B **46** 8219
[52] Arnold Z, Kamarad J, Mikulina O, Garcia-Landa B, Abadia C, Ibarra M R and Kudrevatykh N V 1999 *J. Magn. Magn. Mater.* **196/197** 748
[53] Zhang L Y, Boltich E B, Sinha V K and Wallace W E 1989 *IEEE Trans. Magn.* **25** 3303
[54] Tereshina I S, Nikitin S A, Nikiforov V N, Ponomarenko L A, Verbetsky V N, Salamova A A and Skokov K P 2002 *J. Alloys Compounds* **345** 16
[55] Piquer C, Bartolomé J, Artigas M and Fruchart D 2000 *Phys. Rev.* B **62** 1004
[56] Chaboy J and Piquer C 2002 *Phys. Rev.* B **66** 104433
[57] Wang J L, Campbell S J, Cadogan J M, Tegus O and Edge A V J 2005 *J. Phys.: Condens. Matter* **17** 3689